IVYSPRING INTERNATIONAL PUBLISHER

Theranostics

2014; 4(5):546-555. doi: 10.7150/thno.8159

Research Paper

Longitudinal PET Imaging of Muscular Inflammation Using ^{18}F-DPA-714 and ^{18}F-Alfatide II and Differentiation with Tumors

Chenxi Wu[1, 2], Xuyi Yue[2], Lixin Lang[2], Dale O. Kiesewetter[2], Fang Li[1], Zhaohui Zhu[1]✉, Gang Niu[2], Xiaoyuan Chen[2] ✉

1. Department of Nuclear Medicine, Peking Union Medical College Hospital (PUMCH), Chinese Academy of Medical Sciences & Peking Union Medical College (CAMS & PUMC), Beijing, China.
2. Laboratory of Molecular Imaging and Nanomedicine, National Institute of Biomedical Imaging and Bioengineering (NIBIB), National Institutes of Health (NIH), Bethesda, USA

✉ Corresponding author: **Zhaohui Zhu,** Department of Nuclear Medicine, Peking Union Medical College Hospital, Chinese Academy of Medical Science & Peking Union Medical College, No. 1 Shuaifuyuan, Wangfujing Street, Dongcheng District, Beijing 100730, China. Telephone: 86-10-69154196; E-mail: zhuzhh@pumch.cn. **Xiaoyuan Chen,** Laboratory for Molecular Imaging & Nanomedicine, BG 31 RM 1C22 31 Center Dr Bethesda MD 20814. Telephone: 301-451-4246; Email: shawn.chen@nih.gov

Received: 2013.11.18; Accepted: 2014.01.25; Published: 2014.02.26

Abstract

Aim: ^{18}F-DPA-714 is a PET tracer that recognizes macrophage translocator protein (TSPO), and ^{18}F-Alfatide II (^{18}F-AlF-NOTA-E[PEG$_4$-c(RGDfk)]$_2$) is specific for integrin $\alpha_v\beta_3$. This study aims to apply these two tracers for longitudinal PET imaging of muscular inflammation, and evaluate the value of ^{18}F-DPA-714 in differentiating inflammation from tumor.

Methods: RAW264.7 mouse macrophage cells were used for cell uptake analysis of ^{18}F-DPA-714. A mouse hind limb muscular inflammation model was established by intramuscular injection of turpentine oil. For the inflammation model, PET imaging was performed at different days using ^{18}F-DPA-714 and ^{18}F-Alfatide II. The specificity of the imaging probes was tested by co- or pre-injection of PK11195 or unlabeled RGD (Arg-Gly-Asp) peptide. PET imaging using ^{18}F-DPA-714 was performed in A549, HT29, U87MG, INS-1, and 4T1 xenograft models. Immunofluorescence staining was performed to evaluate infiltrated macrophages and angiogenesis in inflammation and/or tumors.

Results: Uptake of ^{18}F-DPA-714 in RAW264.7 cells was 45.5% at 1 h after incubation, and could be blocked by PK11195. PET imaging showed increased ^{18}F-DPA-714 and ^{18}F-Alfatide II uptake at inflammatory muscles. Peak uptake of ^{18}F-DPA-714 was seen on day 6 (4.02 ± 0.64 %ID/g), and peak uptake of ^{18}F-Alfatide II was shown on day 12 (1.87 ± 0.35 %ID/g) at 1 h p.i.. Tracer uptakes could be inhibited by PK11195 for ^{18}F-DPA-714 or cold RGD for ^{18}F-Alfatide II. Moreover, macrophage depletion with liposomal clodronate also reduced the local accumulation of both tracers. A549, HT29, U87MG, INS-1, and 4T1 tumor uptakes of ^{18}F-DPA-714 (0.46 ± 0.28, 0.91 ± 0.08, 1.69 ± 0.67, 1.13 ± 0.33, 1.22 ± 0.55 %ID/g at 1 h p.i., respectively) were significantly lower than inflammation uptake (All $P < 0.05$).

Conclusion: PET imaging using ^{18}F-DPA-714 as a TSPO targeting tracer could evaluate the dynamics of macrophage activation and infiltration in different stages of inflammatory diseases. The concomitant longitudinal PET imaging with both ^{18}F-DPA-714 and ^{18}F-Alfatide II matched the causal relationship between macrophage infiltration and angiogenesis. Moreover, we found ^{18}F-DPA-714 uptake in several types of tumors is significantly lower than that in inflammatory muscles, suggesting ^{18}F-DPA-714 PET has the potential for better differentiation of tumor and non-tumor inflammation.

Key words: ^{18}F-DPA-714, ^{18}F-Alfatide II, positron emission tomography, inflammation, tumor, TSPO

Introduction

Inflammation is a common pathological process shared by many diseases including metabolic diseases [1], neurodegenerative disorders [2], cardiovascular diseases [3] as well as malignant tumors [4]. Positron emission tomography (PET) using ^{18}F-FDG (2-deoxy-2-^{18}F-fluoro-D-glucose) has been successfully applied in clinics for tumor detection, staging and therapy response monitoring [5]. ^{18}F-FDG PET can also provide useful information to evaluate focal and generalized infectious and inflammatory disorders [6]. However, ^{18}F-FDG PET has its own limitation in differentiating tumors and non-tumor inflammatory diseases [7]. Therefore, intensive effort has been made to identify more tumor specific PET imaging tracers [7]. Vice versa, inflammation specific imaging tracers are also needed to provide more accurate diagnosis of inflammatory diseases and better understanding of the pathological process.

It has been known that macrophage infiltration into inflammatory foci is one key step in inflammation progression [4]. After being activated, the recruited macrophages will act either as defenders against invasive pathogens, or as promoters to stimulate local inflammatory reaction by releasing different types of chemokines and cytokines. In the later phase, macrophages help to attract and activate endothelia cells, resulting in the formation of new blood vessels in inflammatory foci. Therefore, macrophage targeted PET imaging tracers have been developed to evaluate inflammation diseases [8, 9].

One of the macrophage related targets is the translocator protein (TSPO), or formerly known peripheral benzodiazepine receptor (PBR). TSPO is located on the outer mitochondrial membrane of many types of cell including macrophages, neutrophils, and lymphocytes. Recently, TSPO targeted PET has been applied mainly for neuroinflammation imaging such as stroke [10, 11], traumatic brain injury [12] and Alzheimer's disease [13]. PET imaging studies in atherosclerosis inflammation [14, 15] and arthritis [8, 9] have also been reported with TSPO specific tracers. Most studies used the first generation of TSPO targeting PET tracers, such as ^{11}C-PK11195 or ^{11}C-PBR28. However, the short half-live of ^{11}C ($t_{1/2}$ = 20.38 min) and inherent low sensitivity of these tracers greatly hampered their further applications [16]. ^{18}F-DPA-714 is a new generation of TSPO targeting PET tracers, and has been reported to have increased binding affinity, higher signal-to-noise ratio and low lipophilicity [10, 17]. So far, ^{18}F-DPA-714 has been successfully used in many types of neuroinflammatory diseases [10, 11, 17, 18]. However, for inflammation in peripheral tissues, no study has been reported using ^{18}F-DPA-714 PET imaging.

As mentioned above, macrophage also plays a key role in inflammatory angiogenesis in many types of inflammatory diseases, such as arthritis [19] and diabetic retinopathy [20]. Anti-macrophage therapies showed optimistic results in some inflammatory diseases [21]. Therefore, visualization of inflammatory angiogenesis may provide useful information for diagnosis of inflammatory disease as well as for therapy evaluation of anti-macrophage or anti-angiogenesis treatment. RGD peptide with a sequence of three amino acids Arg-Gly-Asp is one integrin $\alpha_v\beta_3$ specific ligand. Radiolabeled RGD has been used extensively for PET imaging tumor angiogenesis [22, 23], but only a few studies were reported in the realm of non-tumor inflammatory diseases [24, 25].

In this study, we performed longitudinal PET imaging using both ^{18}F-DPA-714 and ^{18}F-Alfatide II (^{18}F-AlF-NOTA-E[PEG$_4$-c(RGDfk)]$_2$) in a mouse model of peripheral tissue inflammation. We aimed to monitor the uptake patterns of ^{18}F-DPA-714 in muscular inflammation model, and evaluate the potential of ^{18}F-DPA-714 in differential diagnosis of inflammations and tumors. We also evaluated the value of ^{18}F labeled RGD peptide, in PET imaging of inflammatory angiogenesis, and further investigated the role of macrophage in inducing new blood vessel formation in inflammatory reactions.

Methods

Preparation of Radiotracers

Synthesis of ^{18}F-DPA-714

Automated syntheses of ^{18}F-DPA-714 were carried out using a slightly modified TRACERLab FX-FN module (GE Medical Systems, Germany). In brief, the aqueous solution (typically 200 -400 μL, 103 – 133 mCi) containing [^{18}F] fluoride anions was sucked through the Chromafix® (Macherey-Nagel, prepared by washing with 2 mL of ethanol and then rinsing with 4 mL of water) under vacuum. Trapped ^{18}F-fluoride was eluted from the cartridge and transferred to the reaction vessel with an eluent solution containing K_2CO_3 (3 mg in 300 μL of pure water), acetonitrile (500 μL), and 10 mg of Kryptofix-222 (K_{222}, 4,7,13,16,21,24-hexaoxa-1,10-diazabicyclo [8.8.8] hexacosane). The reaction mixture was evaporated to dryness after addition. Then tosylate substrate (3 - 4 mg) was dissolved in dimethyl sulfoxide (0.6 mL), and the mixture was transferred to the dry ^{18}F-labeled KF-K_{222} complex and allowed to react at 165 ^{o}C for 5 min. On completion, the reaction mixture was diluted with semi-preparative HPLC solvent (2 mL) and passed through a Sep-Pak® light Alumina N cartridge (Waters, prepared by washing with 4 mL of ethanol and then rinsing with 8 mL of water). The crude solu-

tion was injected into a Phenomenex Luna 5 μ C^{18} semi-preparative reversed-phase HPLC column (250 × 10 mm), with a mobile phase of H_2O and acetonitrile (55/45, v/v) at a flow rate of 4.0 mL/min. The retention time (t_R) of ^{18}F-DPA-714 was determined to be 21 min. The final formulation of the tracer is performed automatically using a Sep-Pak® Plus C^{18}-based system. The yield is 24 ± 3% with a specific activity of 41 – 107 GBq/μmol (n = 8). The excess ethanol was removed through rotary evaporation and concentrated to 250 - 350 μL. The tracer was delivered and diluted with PBS for final formulation and animal study.

Synthesis of ^{18}F-Alfatide II

Radiolabeling of Alfatide II was performed with a similar procedure reported previously [26]. The total synthesis time was about 30 min with radiochemical yield of 40-60% and radiochemical purity > 95%. The specific activity was about 14.8-37 GBq/μmol at the end of synthesis based on the amount of peptide used and the amount of radioactivity trapped on the C-18 column.

Cell culture

Mouse macrophage cell line RAW 264.7, human lung carcinoma cell line A549, human colon cancer cell line HT29, human brain glioblastoma cell line U87MG, rat insulinoma cell line INS-1 and mouse breast cancer cell line 4T1 were obtained from the American Type Culture Collection (ATCC, Manassas, VA). RAW 264.7, A549 and 4T1 cells were grown in DMEM culture medium, HT29 and INS-1 cells were grown in RPMI-1640 culture medium, and U87MG cells were grown in MEM culture medium. All culture mediums (Invitrogen, Carlsbad, CA) were supplemented with 10% (v/v) fetal bovine serum (FBS, Invitrogen), 100 IU/ml penicillin and 100 μg/ml streptomycin (Invitrogen) at 37°C in a humidified atmosphere containing 5% CO_2.

Macrophage cell uptake and efflux assay

For cell uptake of ^{18}F-DPA-714 and ^{18}F-Alfatide II, RAW 274.7 cells were seeded into 24-well plates at a density of 1×10^5 cells per well and incubated with 18.5 kBq (0.5 μCi) per well of ^{18}F-DPA-714 (with or without 5ng/ml PK11195 co-culturing for blocking) or ^{18}F-Alfatide II at 37°C for 15, 30, 60, and 120 min. The cells were then washed three times with cold phosphate buffered saline (PBS) and lysed with 500 μl 0.1 N sodium hydroxide (NaOH). The cell lysate in each well were then collected and measured in a γ counter (Wallac Wizard 1480, PerkinElmer Inc.). For efflux studies of ^{18}F-DPA-714, RAW 274.7 cells seeded into 24-well plates were incubated with 18.5 kBq (0.5 μCi) per well of ^{18}F-DPA-714 at 37°C for 120 min. Then cells were washed twice with cold PBS, and incubated with DMEM medium for 15, 30, 60, 120 min. The cells were then washed three times with cold PBS and lysed with 500 μl 0.1 N NaOH for gamma counter measurement. The cell uptake was expressed as the percent added dose (% AD) after decay correction. Experiments were performed in triplicates.

Animal models

The animal study protocol was in accordance with the principles and procedures outlined in the Guide for the Care and Use of Laboratory Animals and approved by the Institutional Animal Care and Use Committee of the Clinical Center, National Institutes of Health (Animal protocol NIBIB 13-01). Mouse hind limb inflammation models and 4T1 xenograft tumor models were prepared in 6-8-wk-old female FVB mice, and A549, HT29, U87MG, INS-1 xenograft tumor models were inoculated in 6-8-wk-old female athymic nude mice. For mouse hind limb muscular inflammation model, 20 μl oil of turpentine (Sigma-Aldrich, USA) was injected into the left thigh muscle of each mouse (day 0) using a 30-gauge hypodermic needle. For tumor models, about 5×10^6 tumor cells of A549, HT29, U87MG, INS-1 and 4T1 were inoculated in mouse flanks respectively. The tumor growth was monitored by caliper measurement and tumor volumes were estimated by the formula of $a\times b^2 / 2$, in which a and b was the length and width of the tumor, respectively, in millimeters. All mice were maintained in the Animal Facility in NIH under specific pathogen-free conditions and a 12h/12h light-dark cycle. Food and water could be accessed *ad-libitum*.

Macrophage depletion

Mouse macrophage depletion was done by intravenous (i.v.) injection of liposomal clodronate (Clophosome, FormuMax Scientific Inc., USA). Three days after turpentine oil injection, mice (two groups, 4 mice in each group) received 1.4 mg (200 μl) liposomal clodronate, and then 0.7 mg (100 μl) every 2-3 days (scheme 1). Another four mice received 1.4 mg (200 μl) liposomal clodronate started 2 days before turpentine oil injection, and then 0.7 mg (100 μl) every 2-3 days (scheme 2).

PET imaging

PET scans and image analysis were performed using an Inveon small animal PET scanner (Siemens Preclinical Solutions). For ^{18}F-DPA-714 static PET imaging, a 10-minute acquisition was performed at 1 h after tail vein injection of about 5.56 MBq (150 μCi) ^{18}F-DPA-714 on day 1, 3, 6, 10, 14, 19 and 26 after turpentine oil injection. For PK11195 displacement of ^{18}F-DPA-714 uptake, 5mg/kg PK11195 (in purified water) were injected via tail vein at 25-min during a

1-h dynamic PET acquisition procedure on day 3. For ^{18}F-Alfatide II PET imaging, a 10-minute acquisition was performed at 1 h after injection of about 5.56 MBq (150 μCi) ^{18}F-Alfatide II on day 1, 2, 4, 8, 12, 16 and 26 after turpentine oil injection. For RGD blocking imaging, unlabeled NOTA-PRGD2 peptide (10 mg/kg) was injected 10 min before ^{18}F-Alfatide II injection on day 9. For PET imaging of macrophage depletion groups, one group of mice under macrophage depletion scheme 1 went through ^{18}F-DPA-714 PET imaging (1 h after tracer inj.) on day 6, 10 and 14 after turpentine oil injection, while the other group of mice under scheme 1 and the group under scheme 2 went through ^{18}F-Alfatide II PET imaging (1 h after tracer inj.) on day 12 after turpentine injection. For A549, HT29, U87MG, INS-1 and 4T1 tumor model mice, ^{18}F-DPA-714 PET imaging was performed at 1 h after tracer injection when the tumor volume reached 100–300 mm^3 (3–5 weeks after inoculation)

The images were reconstructed using a two-dimensional ordered-subsets expectation maximization (2-D OSEM) (for ^{18}F-DPA-714 images) or 3-D OSEM (for ^{18}F-Alfatide II images) algorithm without attenuation or scattering correction. Three-dimensional Regions of Interests (3D-ROIs) were placed on the inflammatory muscles or tumors, and a threshold of 40% of the maximum uptake was used for the final ROI drawing. Assuming a tissue density of 1 g/mL, the radioactivity contained in the ROI was divided by the dose administered to the animal and the volume of the ROI to obtain an imaging ROI-derived % ID/g.

Autoradiography

In vitro autoradiography was performed on cryosecitons of the inflammatory muscle samples collected on day 1, 6 and 22 after turpentine injection. The samples was embedded and frozen in CRYO-OCT compound (Tissue-Tek) and serial 10 μm sections were obtained using a cryostat (UltraPro 5000, Vibratome, St. Louis, MO, USA). Cryosecitons were fixed using buffered zinc formalin fixatives (Z-fix, Anatech Ltd.) for 10 minutes, followed by 5 min PBS wash. Each sample was incubated with 18.5 kBq (0.5 μCi) ^{18}F-DPA-714 with or without PK11195 (50 ng per sample) for 30min in Tris buffer, and then rinsed 2 times with PBS for 2 min each time, followed by a quick wash in distilled water. After quick dry, sections were placed in direct contact with a Phosphor-Imager screen. After overnight exposure, images were developed in a Cyclone Plus Storage Phosphor System (PerkinElmer, Shelton, CT, USA).

Immunohistochemistry

The inflammatory muscles of mice on day 1, 6 and 12 after turpentine injection and A549, HT29, U87MG, INS-1, 4T1 tumors was collected and embedded and frozen in CRYO-OCT compound. Cryosecitons with thickness of 10 μm were fixed in Z-Fix for 10 minutes, then rinsed with PBS and blocked with 2% bovine serum albumin (BSA) for 30 minutes at room temperature. Inflammation muscle slices were incubated with rabbit anti-CD68 antibody (1:100; Abcam, USA) or rat anti-CD31 antibody (1:100, BD Biosciences) or rabbit anti-PBR antibody (1:100; Abcam, USA) over night at 4 ^{o}C. After 10 min PBS wash for 3 times, slices were incubated with Cy3-conjugated anti-rabbit or FITC-conjugated anti-rat secondary antibodies (1:200; Jackson ImmunoResearch Laboratories, West Grove, PA) for 30 min at dark room in room temperature followed by 10 min PBS wash for 3 times. Tumor tissue sections were incubated with rabbit anti-PBR antibody (1:100; Abcam, USA) for 1 h and then with Cy3-conjugated anti-rabbit secondary antibodies (1:200; Jackson ImmunoResearch Laboratories) for 30 min at dark room in room temperature followed by 10 min PBS wash for 3 times. All slices were mounted with VECTASHIELD® mounting medium containing DAPI and covered with cover slides before visualization under an epifluorescence microscopy (IX-81, Olympus).

Statistical analysis

Quantitative data are expressed as mean ± SD. Means were compared using the Student's t test. *P* values of < 0.05 were considered statistically significant.

Results

RAW 264.7 cell uptake and efflux studies

Both ^{18}F-DPA-714 and ^{18}F-Alfatide II were synthesized successfully with high specific activity. Prior to *in vivo* imaging, we evaluated uptake of the tracers in murine macrophage cell line RAW246.7 cells with a standard cell uptake and efflux assay. ^{18}F-DPA-714 showed a very high uptake with the cells and the level reached a maximum of 45.55 ± 0.02 % of added dose (AD) at 1 h time point and kept the similar high level till 2 h. With the presence of PK11195 as a competitor, uptake of ^{18}F-DPA-714 decreased remarkably to 1.27 ± 0.00 %AD at 1 h ($p < 0.001$). The results indicated that ^{18}F-DPA-714 efficiently accumulates in macrophages with high specificity to the target protein TSPO. After 2 h incubation with ^{18}F-DPA-714 and medium change, RAW246.7 cells showed decreased radioactivity retention along with time. However, there is still decent level of tracer retention with 1 h efflux (21.55 ± 2.05 %AD, around 50 %) **(Figure 1A)**. With ^{18}F-Alfatide II, although we observed increased cell uptake along with time, the level was pretty low with the highest

uptake of only 0.18 ± 0.03 % AD at 2 h after incubation **(Figure 1B)**.

Longitudinal PET imaging of muscular inflammation

Next we performed longitudinal PET imaging in a turpentine induced mouse muscular inflammation model using ^{18}F-DPA-714 to target TSPO and ^{18}F-Alfatide II to evaluate angiogenesis. As shown in **Figure 2A&B**, after turpentine injection, the inflammatory muscles showed significantly increased local accumulation of ^{18}F-DPA-714 compared with the collateral muscle. The uptake peaked on day 6 (4.02 ± 0.64 %ID/g), then dropped slowly along with time till day 26, which was still higher than that in collateral muscle. We also performed 1 h dynamic ^{18}F-DPA-714 PET imaging with PK11195 displacement on day 3 after turpentine injection. Reflected by the time activity curves (TACs), ^{18}F-DPA-714 uptake was significantly displaced by a blocking dose of PK11195 (5mg/kg) at 25 min after ^{18}F-DPA-714 injection, while the contralateral normal muscle stayed at the same low uptake level, unaffected by PK11195 injection **(Figure 2C, D)**. The results further confirmed the specificity of ^{18}F-DPA-714 for TSPO evaluation.

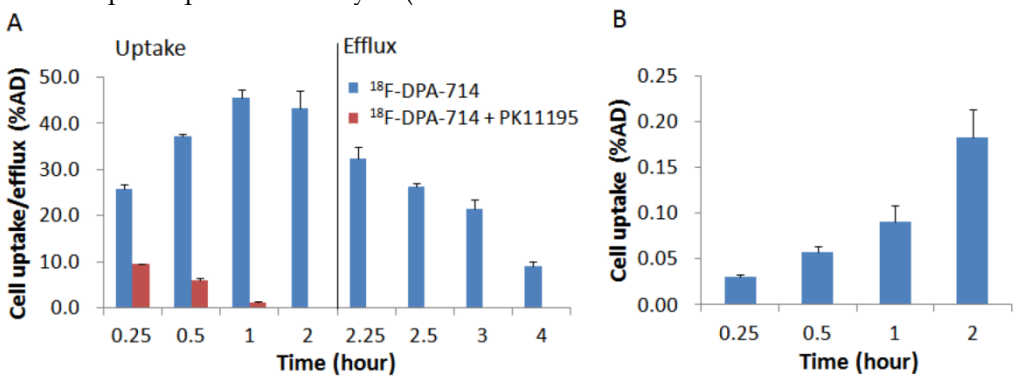

Figure 1. (A) Cell uptake and efflux of ^{18}F-DPA-714 in RAW264.7 cells with or without blocking agent PK11195 (n = 3, mean ± SD). (B) Cell uptake of ^{18}F-Alfatide II in RAW264.7 cells (n = 3, mean ± SD).

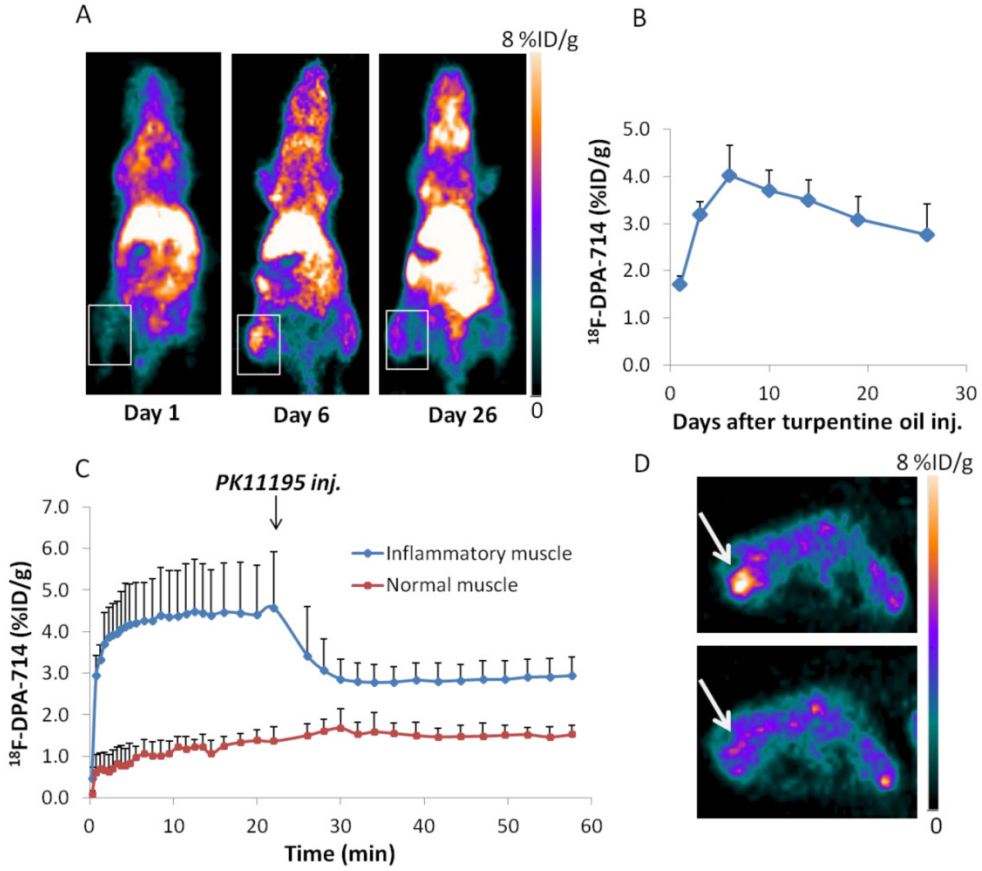

Figure 2. (A) ^{18}F-DPA-714 PET imaging of mouse muscular inflammation model on day 1, 6 and 26 after turpentine oil injection. White boxes indicate inflammatory muscles. (B) PET images based quantitative analysis of ^{18}F-DPA-714 uptake in inflammatory muscles on day 1, 3, 6, 10, 14, 19 and 26 after turpentine oil injection. Peak uptake was seen on day 6 (4.02 ± 0.64 %ID/g). (C) Time activity curves (TACs) of inflammatory muscles from 1 h ^{18}F-DPA-714 dynamic PET imaging with PK11195 displacement. (D) Representative transaxial PET images of ^{18}F-DPA-714 uptake in inflammatory muscle before and after K11195 displacement.

To confirm *in vivo* PET imaging, we also performed *in vitro* ^{18}F-DPA-714 autoradiography with inflammatory muscle samples. The autoradiograph results showed similar trend with PET imaging. Moreover, ^{18}F-DPA-714 uptake by all inflammatory muscle samples could be blocked by co-incubation with PK11195 **(Supplementary Material: Figure S1)**. We also evaluated macrophage infiltration in inflammatory samples by immunostaining of the macrophage marker, CD68. Sections of inflammatory muscles obtained at day 6 **(Supplementary Material: Figure S2B)** after turpentine injection showed higher degree of CD68 staining of macrophage compared to day 1 (**Supplementary Material: Figure S2A**). Sections of day 6 inflammatory muscles under macrophage depletion treatment (**Supplementary Material: Figure S2C**) showed lower CD68 staining signal compared to day 6 inflammations without macrophage depletion.

For ^{18}F-Alfatide II PET imaging, the inflammatory muscle also showed increased local accumulation. The highest ^{18}F-Alfatide II uptake was seen on day 12 (1.87 ± 0.35 %ID/g) after turpentine injection **(Figure 3A, B)**, which is about 6 days later than that of ^{18}F-DPA-714. ^{18}F-Alfatide II uptake in inflammatory muscles could be blocked by unlabeled dimeric RGD peptide administered 10 min before tracer injection **(Figure 3C, D)**. The increased angiogenesis was confirmed with immunofluorescence staining against CD31, an endothelial cell marker. The fluorescence signal in inflammatory muscle sections obtained on day 12 after turpentine injection is much higher than that in samples obtained on day 1 (**Supplementary Material: Figure S2D, E**).

PET imaging of inflammation after macrophage depletion

Since TSPO is overexpressed on macrophages, it is reasonable to deduce that the high uptake of ^{18}F-DPA-714 in inflammatory muscles is macrophage related. Therefore, we performed ^{18}F-DPA-714 PET after macrophage depletion with i.v. injection of liposomal clodronate. With treatment scheme 1, uptake of ^{18}F-DPA-714 in inflammatory muscles was significantly lower on day 6 and day 10 compared to that in untreated mice at the same day (3.30 ± 0.18 v.s. 4.02 ± 0.64 %ID/g, P = 0.02 and 3.16 ± 0.32 v.s. 3.70 ± 0.43 %ID/g, P = 0.03, respectively). However, on day 14 after turpentine injection, no significant difference of ^{18}F-DPA-714 in inflammatory muscles was observed **(Figure 4A)**.

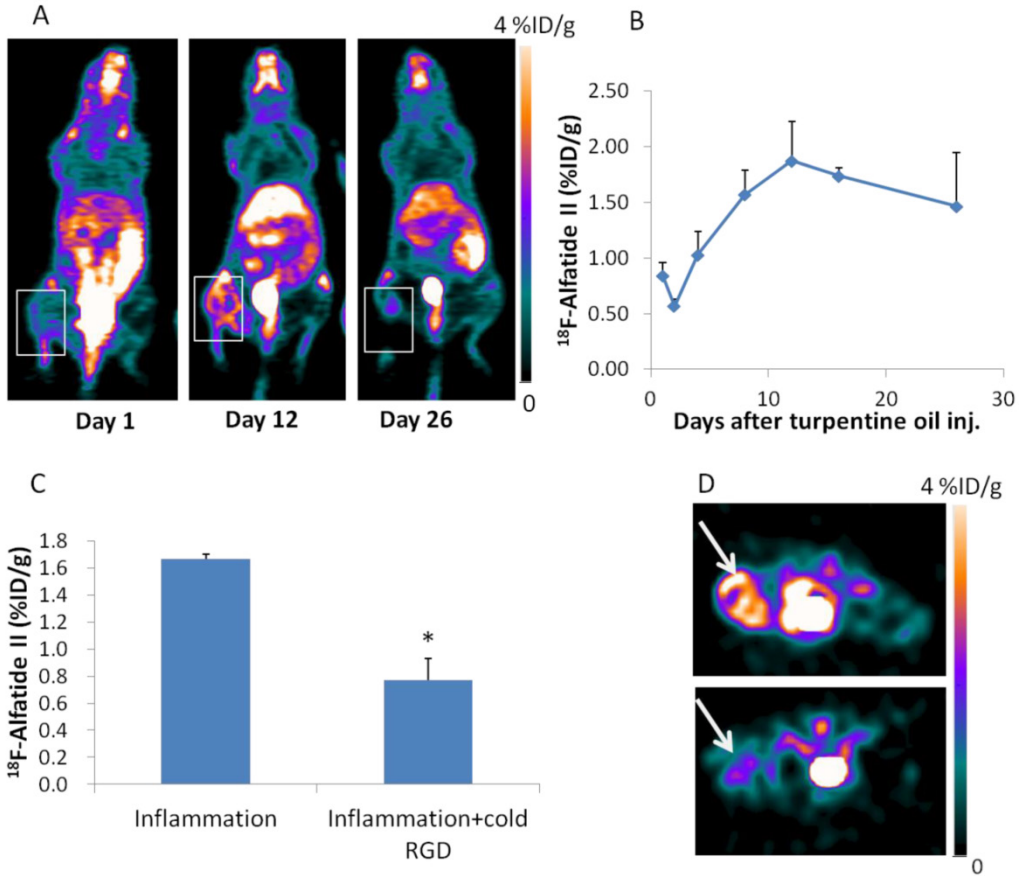

Figure 3. (A) ^{18}F-Alfatide II PET imaging of mouse muscular inflammation model on day 1, 12 and 26 after turpentine oil injection. White boxes indicate inflammatory muscles. (B) PET images based quantitative analysis of ^{18}F-Alfatide II uptake in inflammatory muscles on day 1, 2, 4, 8, 12, 16 and 26 after turpentine oil injection. Peak uptake was seen on day 12 (1.87 ± 0.35 %ID/g). (C) Quantification of ^{18}F-Alfatide II uptake in inflammatory muscles on day 9 after turpentine injection with or without cold RGD blocking. (D) Representative transaxial PET images of ^{18}F-Alfatide II uptake in inflammatory muscle without and with cold RGD blocking.

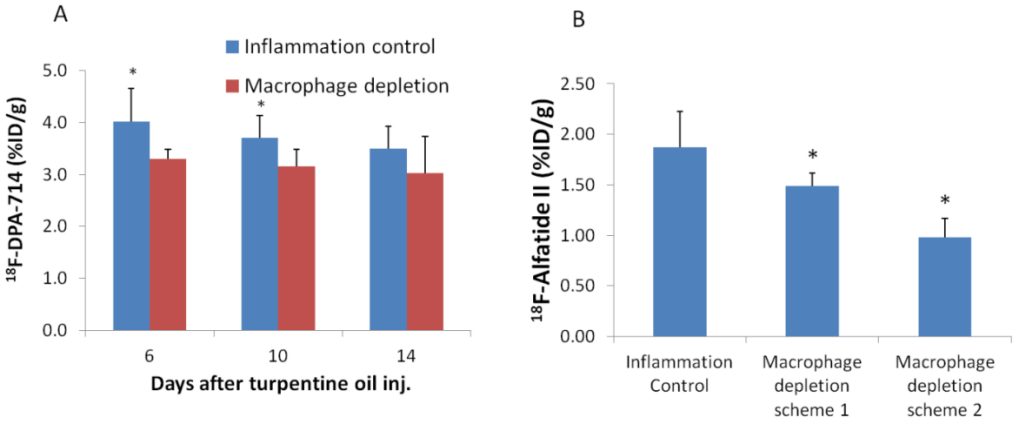

Figure 4. (A) PET imaging based quantification of ^{18}F-DPA-714 uptake in inflammatory muscles at day 6, 10 and 14 after turpentine oil injection with or without macrophage depletion. The mice received 1.4mg (200μl) liposomal clodronate on day 3 after turpentine oil injection and then 0.7 mg (100 μl) every 2-3 days (Scheme 1). (B) Quantification of ^{18}F-Alfatide II uptake in inflammatory muscles on day 12 after turpentine oil injection under different macrophage depletion methods. Mice with treatment scheme 2 (1.4 mg liposomal clodronate started 2 days before turpentine oil injection and then 0.7 mg every 2-3 days) showed even lower uptake compared to mice with treatment scheme 1 (1.4 mg liposomal clodronate started on day 3 and then 0.7 mg every 2-3 days).

After macrophage depletion by scheme 1, inflammatory uptake of ^{18}F-Alfatide II was also significant decreased on day 12 compared to that in untreated mice at the same day (1.49 ± 0.13 v.s. 1.87 ± 0.35 %ID/g, P = 0.03). Under macrophage depletion scheme 2, the uptake was even lowered (0.98 ± 0.19 v.s. 1.87 ± 0.35 %ID/g, $P = 2.97\times10^{-4}$) **(Figure 4B)**. The effect of macrophage depletion on inflammatory angiogenesis was further confirmed by immunostaining against CD31. Sections of day 12 inflammatory muscles under macrophage depletion showed lower CD31 staining signal compared to day 12 inflammations without macrophage depletion (**Supplementary Material: Figure S2E, F**)

^{18}F-DPA-714 PET imaging of tumors

Macrophage infiltration is also well-known in solid tumors, thus we chose several tumor models and performed PET imaging with ^{18}F-DPA-714. As shown in **Figure 5**, ^{18}F-DPA-714 showed variant uptake in different types of tumor. Among them, A549 tumors showed the lowest uptake with a value of 0.46 ± 0.28 %ID/g. U87MG tumors showed the highest ^{18}F-DPA-714 accumulation (1.69 ± 0.67 %ID/g). HT29, INS-1 and 4T1 showed similar uptake value in between (0.91 ± 0.08, 1.13 ± 0.33, 1.22 ± 0.55 %ID/g, respectively). All these values were significantly lower than that in inflammatory muscles from day 3 to day 26 after turpentine injection. Immunofluorescence staining against TSPO in these tumor sections also showed much lower fluorescence signal than inflammatory muscle sections obtained on day 7 after turpentine injection (**Supplementary Material: Figure S3**).

Discussion

As a new generation of TSPO targeted radioligand, ^{18}F-DPA-714 has been mainly used in PET imaging of neuroinflammatory diseases [10, 11, 17, 18]. To the best of our knowledge, ^{18}F-DPA-714 has not been applied to image peripheral tissue inflammatory diseases, although PET studies in atherosclerosis inflammation [14, 15] and arthritis [8, 9] have been reported with some other types of TSPO specific tracers. In this study, by using a mouse model of muscular inflammation induced by turpentine oil, we investigated the feasibility of ^{18}F-DPA-714 PET in evaluation of peripheral tissue inflammations. We found that ^{18}F-DPA-714 showed specific uptake in inflammatory muscles, especially after day 3 upon turpentine oil injection. This uptake trend was in accordance with the time window of macrophage infiltration into inflammatory foci. Because focal turpentine oil acted as constant stimuli which was difficult to be eliminated by inflammatory cells, inflammatory muscle would turn to chronic inflammation at day 3-6 post inflammation modeling [27]. In acute inflammation phase which is 1-2 days after turpentine oil injection, lymphocytes and neutrophils are the major cell population within inflammatory foci. These cells will change to monocyte/macrophage lineage during chronic inflammatory phase [28]. Therefore, ^{18}F-DPA-714 uptake reached the peak level on day 6, while tracer accumulation was low on day 1 after turpentine oil injection. Combined with the confirmative data from immunostainging and autoradiography, we demonstrated that longitudinal PET imaging with ^{18}F-DPA-714 reflected the dynamic of macrophage infiltration during the inflammatory reaction.

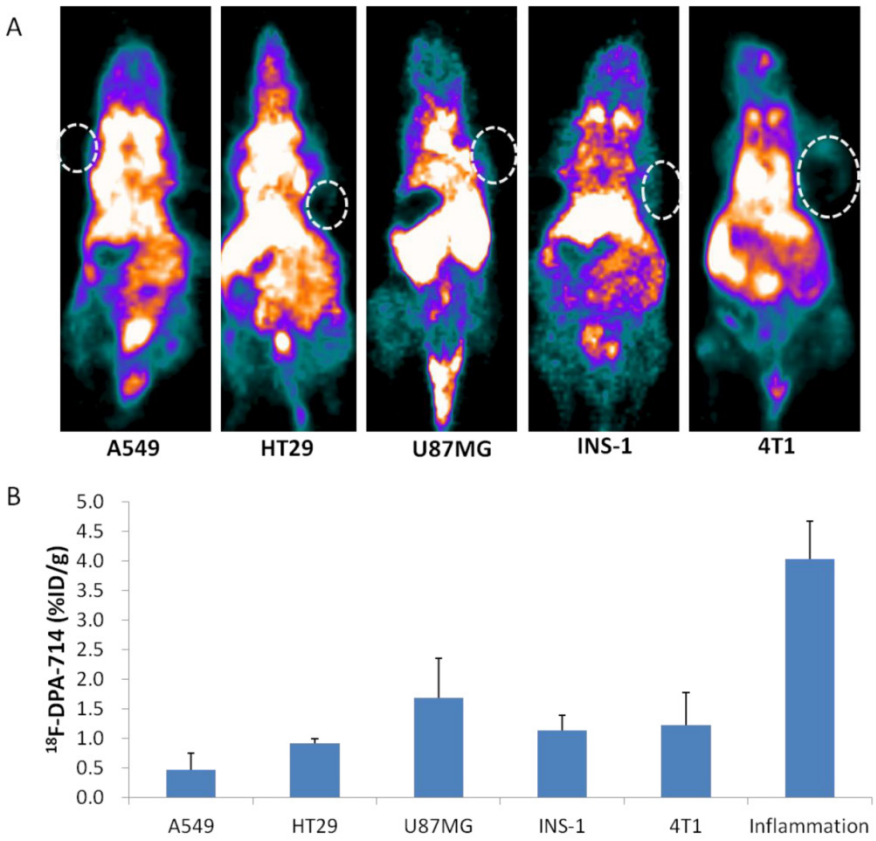

Figure 5. (A) ^{18}F-DPA-714 PET imaging of mice bearing A549, HT29, U87MG, INS-1, 4T1 tumors. (B) Quantitative analysis of different tumor uptakes of ^{18}F-DPA-714 compared to inflammation ^{18}F-DPA-714 uptake on day 6 after turpentine injection.

Liposomal clodronate is widely used as a macrophage depletion agent in many types of inflammatory conditions [29, 30]. Using i.v. injection of liposomal clodronate, it was supposed to deplete the whole body macrophages including those infiltrated into inflammatory muscles [31]. With lower level of macrophage in inflammatory muscle, our imaging successfully showed the decreased level of ^{18}F-DPA-714 uptake within inflammation foci, further suggesting ^{18}F-DPA-714 was targeted to infiltrated macrophages in the inflamed muscles. Macrophage depletion has been an effective way of treating certain inflammatory diseases [32-34]. Our study may provide the feasibility of using TSPO targeted PET imaging to monitor macrophage depletion in muscular inflammation.

TSPO specificity of ^{18}F-DPA-714 was further confirmed by PK11195 displacement as well as *in vitro* autoradiography study using PK11195 as a blocking agent. ^{18}F-DPA-714 binding was rapidly displaced from the inflammatory muscle by an excess amount of PK11195. However, after displacement, ^{18}F-DPA-714 uptake in inflammatory muscles was still higher than that in normal muscles (2.91 ± 0.45 %ID/g and 1.47 ± 0.24 %ID/g, respectively, $P < 0.04$), indicating the displacement was incomplete. This phenomenon may be explained by the lower binding affinity of PK11195 to macrophage TSPO [18]. Besides, it is not clear whether PK11195 and DPA-714 share the exactly same binding site on TSPO.

Chronic inflammation and angiogenesis is interrelated. In chronic inflammation phase, more vasculature is formed under the influence of various angiogenic cytokines and chemokines released from infiltrated lymphocytes [35]. Several anti-macrophage treatments have been investigated in different inflammatory disorders including arthritis [32, 36], encephalomyelitis [33], and colitis [34]. Many of those macrophage related therapies actually took into effects through anti-angiogenesis. In this study, we found that uptake of ^{18}F-Alfatide II showed similar trend with that of ^{18}F-DPA-714 in this inflammation model but with a delayed peak time (12 days v.s. 6 days). In fact, the imaging result from ^{18}F-Alfatide II was consistent with that we reported before in a mouse ear inflammation model [24]. The concomitant longitudinal PET imaging with both ^{18}F-DPA-714 and ^{18}F-Alfatide II in this study may provide help to reveal the causal relationship between macrophage infiltration and angiogenesis. Meanwhile, we found inflammatory angiogenesis was prohibited after macrophage depletion, and different treatment scheme may induce different extent of angiogenesis prohibition. In mice receiving macrophage depletion started

2 days before turpentine oil injection (scheme 2), the inflammatory muscles showed lower ^{18}F-Alfatide II uptake compared to that in mice receiving macrophage depletion started on day 3 after turpentine oil injection (scheme 1). It is possible that macrophage depletion before inflammation occurrence might probably pre-condition the whole environment for future inflammation progression, causing even less macrophage infiltration and inflammatory angiogenesis afterwards. It is foreseeable that one major potential application of these imaging strategies is to provide guidance for anti-macrophage drug development and therapy response monitoring.

In addition to macrophages, TSPO levels are also elevated in many types of cancer cells and tumors including breast, ovary, colon and prostate cancer [37]. Using immunohistochemistry and autoradiography, one study reported moderate to high TSPO expression level in some breast cancer cells as well as tumor stromal cells, indicating a mixed TSPO expression pattern within tumors [38]. However, in this study, all five types of tumors showed very low tumor uptake of ^{18}F-DPA-714 (from 0.46 ± 0.28 to 1.69 ± 0.67 %ID/g), which were significantly lower than inflammatory muscle uptake from day 3 to day 26 after turpentine oil injection (from 2.77 ± 0.64 to 4.02 ± 0.64 %ID/g). One possible explanation is that majority of tumor associated macrophages are M2-polorized [39] and show different phenotype from the classically-activated type 1 macrophages (M1) [40]. Therefore, ^{18}F-DPA-714 seemed to have the potential of differentiating tumors from other inflammatory diseases, although further substantiation is still needed.

Conclusion

In this study, we performed longitudinal PET imaging using ^{18}F-DPA-714 and ^{18}F-Alfatide II to evaluate macrophage infiltration and inflammatory angiogenesis in a mouse model of muscular inflammation. We also evaluated the differential diagnostic ability of ^{18}F-DPA-714 PET in tumor and non-tumor inflammatory lesions. The results supported the feasibility of ^{18}F-DPA-714 as a TSPO targeting tracer to monitor the dynamics of macrophage activation and infiltration in different stages of inflammatory diseases. The concomitant longitudinal PET imaging with both ^{18}F-DPA-714 and ^{18}F-Alfatide II matched the causal relationship between macrophage infiltration and angiogenesis. Moreover, we found ^{18}F-DPA-714 uptake in several types of tumors is significantly lower than that in inflammatory muscles, suggesting ^{18}F-DPA-714 PET has the potential for better differentiation of tumor and non-tumor inflammation.

Supplementary Material

Fig.S1 - S3. http://www.thno.org/v04p0546s1.pdf

Acknowledgements

This work was supported by Department of Nuclear Medicine, Peking Union Medical College Hospital (PUMCH), and the Intramural Research Program (IRP) of the National Institute of Biomedical Imaging and Bioengineering (NIBIB), National Institutes of Health (NIH).

Competing Interests

The authors have declared that no competing interest exists.

References

1. Hotamisligil GS. Inflammation and metabolic disorders. Nature. 2006; 444: 860-7. doi:10.1038/nature05485.
2. Wyss-Coray T, Mucke L. Inflammation in neurodegenerative disease--a double-edged sword. Neuron. 2002; 35: 419-32.
3. Libby P. Inflammation and cardiovascular disease mechanisms. Am J Clin Nutr. 2006; 83: 456S-60S.
4. Coussens LM, Werb Z. Inflammation and cancer. Nature. 2002; 420: 860-7. doi:10.1038/nature01322.
5. Kostakoglu L, Agress H, Jr., Goldsmith SJ. Clinical role of FDG PET in evaluation of cancer patients. Radiographics : a review publication of the Radiological Society of North America, Inc. 2003; 23: 315-40; quiz 533. doi:10.1148/rg.232025705.
6. Haroon A, Zumla A, Bomanji J. Role of fluorine 18 fluorodeoxyglucose positron emission tomography-computed tomography in focal and generalized infectious and inflammatory disorders. Clinical infectious diseases : an official publication of the Infectious Diseases Society of America. 2012; 54: 1333-41. doi:10.1093/cid/cis193.
7. van Waarde A, Cobben DC, Suurmeijer AJ, Maas B, Vaalburg W, de Vries EF, et al. Selectivity of 18F-FLT and 18F-FDG for differentiating tumor from inflammation in a rodent model. J Nucl Med. 2004; 45: 695-700.
8. van der Laken CJ, Elzinga EH, Kropholler MA, Molthoff CF, van der Heijden JW, Maruyama K, et al. Noninvasive imaging of macrophages in rheumatoid synovitis using 11C-(R)-PK11195 and positron emission tomography. Arthritis Rheum. 2008; 58: 3350-5. doi:10.1002/art.23955.
9. Gent YY, Voskuyl AE, Kloet RW, van Schaardenburg D, Hoekstra OS, Dijkmans BA, et al. Macrophage positron emission tomography imaging as a biomarker for preclinical rheumatoid arthritis: findings of a prospective pilot study. Arthritis Rheum. 2012; 64: 62-6. doi:10.1002/art.30655.
10. Boutin H, Prenant C, Maroy R, Galea J, Greenhalgh AD, Smigova A, et al. [18F]DPA-714: direct comparison with [11C]PK11195 in a model of cerebral ischemia in rats. PLoS One. 2013; 8: e56441. doi:10.1371/journal.pone.0056441.
11. Harhausen D, Sudmann V, Khojasteh U, Muller J, Zille M, Graham K, et al. Specific imaging of inflammation with the 18 kDa translocator protein ligand DPA-714 in animal models of epilepsy and stroke. PLoS One. 2013; 8: e69529. doi:10.1371/journal.pone.0069529.
12. Yu I, Inaji M, Maeda J, Okauchi T, Nariai T, Ohno K, et al. Glial cell-mediated deterioration and repair of the nervous system after traumatic brain injury in a rat model as assessed by positron emission tomography. J Neurotrauma. 2010; 27: 1463-75. doi:10.1089/neu.2009.1196.
13. Maeda J, Zhang MR, Okauchi T, Ji B, Ono M, Hattori S, et al. In vivo positron emission tomographic imaging of glial responses to amyloid-beta and tau pathologies in mouse models of Alzheimer's disease and related disorders. J Neurosci. 2011; 31: 4720-30. doi:10.1523/JNEUROSCI.3076-10.2011.
14. Gaemperli O, Shalhoub J, Owen DR, Lamare F, Johansson S, Fouladi N, et al. Imaging intraplaque inflammation in carotid atherosclerosis with 11C-PK11195 positron emission tomography/computed tomography. Eur Heart J. 2012; 33: 1902-10. doi:10.1093/eurheartj/ehr367.
15. Lamare F, Hinz R, Gaemperli O, Pugliese F, Mason JC, Spinks T, et al. Detection and quantification of large-vessel inflammation with 11C-(R)-PK11195 PET/CT. J Nucl Med. 2011; 52: 33-9. doi:10.2967/jnumed.110.079038.
16. Chauveau F, Boutin H, Van Camp N, Dolle F, Tavitian B. Nuclear imaging of neuroinflammation: a comprehensive review of [11C]PK11195 challengers. Eur J Nucl Med Mol Imaging. 2008; 35: 2304-19. doi:10.1007/s00259-008-0908-9.
17. Doorduin J, Klein HC, Dierckx RA, James M, Kassiou M, de Vries EF. [11C]-DPA-713 and [18F]-DPA-714 as new PET tracers for TSPO: a comparison with [11C]-(R)-PK11195 in a rat model of herpes encephalitis. Mol Imaging Biol. 2009; 11: 386-98. doi:10.1007/s11307-009-0211-6.

18. Chauveau F, Van Camp N, Dolle F, Kuhnast B, Hinnen F, Damont A, et al. Comparative evaluation of the translocator protein radioligands 11C-DPA-713, 18F-DPA-714, and 11C-PK11195 in a rat model of acute neuroinflammation. J Nucl Med. 2009; 50: 468-76. doi:10.2967/jnumed.108.058669.
19. Kinne RW, Brauer R, Stuhlmuller B, Palombo-Kinne E, Burmester GR. Macrophages in rheumatoid arthritis. Arthritis Res. 2000; 2: 189-202. doi:10.1186/ar86.
20. Meleth AD, Agron E, Chan CC, Reed GF, Arora K, Byrnes G, et al. Serum inflammatory markers in diabetic retinopathy. Invest Ophthalmol Vis Sci. 2005; 46: 4295-301. doi:10.1167/iovs.04-1057.
21. Lue H, Kleemann R, Calandra T, Roger T, Bernhagen J. Macrophage migration inhibitory factor (MIF): mechanisms of action and role in disease. Microbes Infect. 2002; 4: 449-60.
22. Beer AJ, Kessler H, Wester HJ, Schwaiger M. PET Imaging of Integrin alphaVbeta3 Expression. Theranostics. 2011; 1: 48-57.
23. Lee J, Lee TS, Ryu J, Hong S, Kang M, Im K, et al. RGD peptide-conjugated multimodal NaGdF4:Yb3+/Er3+ nanophosphors for upconversion luminescence, MR, and PET imaging of tumor angiogenesis. J Nucl Med. 2013; 54: 96-103. doi:10.2967/jnumed.112.108043.
24. Cao Q, Cai W, Li ZB, Chen K, He L, Li HC, et al. PET imaging of acute and chronic inflammation in living mice. Eur J Nucl Med Mol Imaging. 2007; 34: 1832-42. doi:10.1007/s00259-007-0451-0.
25. Laitinen I, Saraste A, Weidl E, Poethko T, Weber AW, Nekolla SG, et al. Evaluation of alphavbeta3 integrin-targeted positron emission tomography tracer 18F-galacto-RGD for imaging of vascular inflammation in atherosclerotic mice. Circ Cardiovasc Imaging. 2009; 2: 331-8. doi:10.1161/CIRCIMAGING.108.846865.
26. Guo J, Lang L, Hu S, Guo N, Zhu L, Sun Z, et al. Comparison of Three Dimeric F-AlF-NOTA-RGD Tracers. Mol Imaging Biol. 2013. doi:10.1007/s11307-013-0668-1.
27. Hamazawa Y, Koyama K, Okamura T, Wada Y, Wakasa T, Okuma T, et al. Comparison of dynamic FDG-microPET study in a rabbit turpentine-induced inflammatory model and in a rabbit VX2 tumor model. Ann Nucl Med. 2007; 21: 47-55.
28. Feghali CA, Wright TM. Cytokines in acute and chronic inflammation. Front Biosci. 1997; 2: d12-26.
29. Koneru R, Kobiler D, Lehrer S, Li J, van Rooijen N, Banerjee D, et al. Macrophages play a key role in early blood brain barrier reformation after hypothermic brain injury. Neurosci Lett. 2011; 501: 148-51. doi:10.1016/j.neulet.2011.06.062.
30. Villalta SA, Rinaldi C, Deng B, Liu G, Fedor B, Tidball JG. Interleukin-10 reduces the pathology of mdx muscular dystrophy by deactivating M1 macrophages and modulating macrophage phenotype. Hum Mol Genet. 2011; 20: 790-805. doi:10.1093/hmg/ddq523.
31. Tidball JG, Wehling-Henricks M. Macrophages promote muscle membrane repair and muscle fibre growth and regeneration during modified muscle loading in mice in vivo. J Physiol. 2007; 578: 327-36. doi:10.1113/jphysiol.2006.118265.
32. Li J, Hsu HC, Yang P, Wu Q, Li H, Edgington LE, et al. Treatment of arthritis by macrophage depletion and immunomodulation: testing an apoptosis-mediated therapy in a humanized death receptor mouse model. Arthritis Rheum. 2012; 64: 1098-109. doi:10.1002/art.33423.
33. Denkinger CM, Denkinger M, Kort JJ, Metz C, Forsthuber TG. In vivo blockade of macrophage migration inhibitory factor ameliorates acute experimental autoimmune encephalomyelitis by impairing the homing of encephalitogenic T cells to the central nervous system. J Immunol. 2003; 170: 1274-82.
34. Ohkawara T, Nishihira J, Takeda H, Hige S, Kato M, Sugiyama T, et al. Amelioration of dextran sulfate sodium-induced colitis by anti-macrophage migration inhibitory factor antibody in mice. Gastroenterology. 2002; 123: 256-70.
35. Wu C, Li F, Niu G, Chen X. PET imaging of inflammation biomarkers. Theranostics. 2013; 3: 448-66. doi:10.7150/thno.6592.
36. Howard KA, Paludan SR, Behlke MA, Besenbacher F, Deleuran B, Kjems J. Chitosan/siRNA nanoparticle-mediated TNF-alpha knockdown in peritoneal macrophages for anti-inflammatory treatment in a murine arthritis model. Mol Ther. 2009; 17: 162-8. doi:10.1038/mt.2008.220.
37. Black KL, Ikezaki K, Santori E, Becker DP, Vinters HV. Specific high-affinity binding of peripheral benzodiazepine receptor ligands to brain tumors in rat and man. Cancer. 1990; 65: 93-7.
38. Zheng J, Boisgard R, Siquier-Pernet K, Decaudin D, Dolle F, Tavitian B. Differential expression of the 18 kDa translocator protein (TSPO) by neoplastic and inflammatory cells in mouse tumors of breast cancer. Mol Pharm. 2011; 8: 823-32. doi:10.1021/mp100433c.
39. Schmieder A, Michel J, Schonhaar K, Goerdt S, Schledzewski K. Differentiation and gene expression profile of tumor-associated macrophages. Seminars in cancer biology. 2012; 22: 289-97. doi:10.1016/j.semcancer.2012.02.002.
40. Quatromoni JG, Eruslanov E. Tumor-associated macrophages: function, phenotype, and link to prognosis in human lung cancer. American journal of translational research. 2012; 4: 376-89.